

Attenuation and Restoration of Severe Acute Respiratory Syndrome Coronavirus Mutant Lacking 2'-O-Methyltransferase Activity

Vineet D. Menachery,^a Boyd L. Yount, Jr.,^a Laurence Josset,^c Lisa E. Gralinski,^a Trevor Scobey,^a Sudhakar Agnihothram,^a Michael G. Katze,^{c,d} Ralph S. Baric^{a,b}

Departments of Epidemiology^a and Microbiology and Immunology,^b University of North Carolina, Chapel Hill, North Carolina, USA; Department of Microbiology, School of Medicine, University of Washington, Seattle, Washington, USA^c; Washington National Primate Research Center, University of Washington, Seattle, Washington, USA^d

ABSTRACT

The sudden emergence of severe acute respiratory syndrome coronavirus (SARS-CoV) in 2002 and, more recently, Middle Eastern respiratory syndrome CoV (MERS-CoV) underscores the importance of understanding critical aspects of CoV infection and pathogenesis. Despite significant insights into CoV cross-species transmission, replication, and virus-host interactions, successful therapeutic options for CoVs do not yet exist. Recent identification of SARS-CoV NSP16 as a viral 2'-O-methyltransferase (2'-O-MTase) led to the possibility of utilizing this pathway to both attenuate SARS-CoV infection and develop novel therapeutic treatment options. Mutations were introduced into SARS-CoV NSP16 within the conserved KDKE motif and effectively attenuated the resulting SARS-CoV mutant viruses both *in vitro* and *in vivo*. While viruses lacking 2'-O-MTase activity had enhanced sensitivity to type I interferon (IFN), they were not completely restored in their absence *in vivo*. However, the absence of either MDA5 or IFIT1, IFN-responsive genes that recognize unmethylated 2'-O RNA, resulted in restored replication and virulence of the dNSP16 mutant virus. Finally, using the mutant as a live-attenuated vaccine showed significant promise for possible therapeutic development against SARS-CoV. Together, the data underscore the necessity of 2'-O-MTase activity for SARS-CoV pathogenesis and identify host immune pathways that mediate this attenuation. In addition, we describe novel treatment avenues that exploit this pathway and could potentially be used against a diverse range of viral pathogens that utilize 2'-O-MTase activity to subvert the immune system.

IMPORTANCE

Preventing recognition by the host immune response represents a critical aspect necessary for successful viral infection. Several viruses, including SARS-CoV, utilize virally encoded 2'-O-MTases to camouflage and obscure their viral RNA from host cell sensing machinery, thus preventing recognition and activation of cell intrinsic defense pathways. For SARS-CoV, the absence of this 2'-O-MTase activity results in significant attenuation characterized by decreased viral replication, reduced weight loss, and limited breathing dysfunction in mice. The results indicate that both MDA5, a recognition molecule, and the IFIT family play an important role in mediating this attenuation with restored virulence observed in their absence. Understanding this virus-host interaction provided an opportunity to design a successful live-attenuated vaccine for SARS-CoV and opens avenues for treatment and prevention of emerging CoVs and other RNA virus infections.

Coronaviruses (CoVs) are large enveloped RNA viruses that primarily infect mammals and birds causing a range of economically significant respiratory and enteric diseases (1). Human CoVs cause medically relevant respiratory tract infections, and most originated as zoonosis from bats (2). In 2003–2004, severe acute respiratory syndrome CoV (SARS-CoV) emerged from CoVs circulating between bats, civets, and raccoon dogs in open markets causing severe acute respiratory disease with mortality rates exceeding 50% in aged populations (3, 4). Although numerous insights into CoV pathogenesis have been developed, the virus host-interactions that regulate disease severity remain poorly understood. In addition, the presence of CoV precursors in animal reservoirs highlights the possibility of future emergent epidemic strains as demonstrated by the recent emergence of Middle East respiratory syndrome CoV in 2012 (5–10). Together, these factors illustrate the need to understand the molecular mechanisms that regulate and permit emerging virus infection, cross-species transmission, and pathogenesis.

One area of interest involves transcription and translation of viral mRNA during infection. Eukaryotic host mRNAs possess a 5'-terminal cap essential for efficient export, translation, and sta-

bility. Naturally, viral pathogens have coevolved mechanisms to replicate this cap structure, thus permitting the use of the host cell translational machinery and efficient replication (11–15). Approaches vary from utilization of the host capping machinery to cap-snatching from host RNA (16). For many cytoplasmic RNA viruses, significant genetic capital has been invested in viral proteins that facilitate proper capping of viral mRNA. For CoVs, several highly conserved nonstructural proteins (NSPs) have been implicated in viral RNA capping activity, including NSP13 (RTPase) (17, 18), NSP14 (N7-methyltransferase [N7-MTase]) (19), and the NSP10/NSP16 2'-O-methyltransferase (2'-O-MTase) complex (20–25). Although N7 methylation has been

Received 16 December 2013 Accepted 22 January 2014

Published ahead of print 29 January 2014

Editor: T. S. Dermody

Address correspondence to Ralph S. Baric, rbaric@email.unc.edu.

Copyright © 2014, American Society for Microbiology. All Rights Reserved.

doi:10.1128/JVI.03571-13

shown to be important in a variety of mRNA processing aspects, the role of 2'-O methylation had been unclear (12). Recent reports, however, detailed a role for 2'-O methylation in distinguishing self from nonself RNA within the host (12, 26). Therefore, by encoding an active 2'-O-MTase in combination with other capping features, viruses can subvert host recognition of their mRNA and fail to induce a strong cell intrinsic immune response.

The host response to infection begins with recognition of viral intermediates by sensor molecules that induce type I interferon (IFN); IFN signaling then regulates infection through production of several hundred interferon-stimulated genes (ISGs) that initiate an antiviral state and limit virus replication (27–29). The discovery of 2'-O methylation in distinguishing between self and non-self RNA accelerated interest in ISGs that target the absence of this motif. MDA5, a RIG-I like molecule, has been shown to recognize unmethylated 2'-O RNA and stimulate type I IFN (12). Similarly, the IFIT family proteins have also been shown to recognize capped RNA without 2'-O methylation but instead may sequester target RNA, thus blocking translation (26). Each ISG is strongly induced during infection, but viruses have evolved mechanisms to circumvent this type of recognition (11, 12, 30). However, absent these strategies, viruses would likely be sensitive to the effector activities that target unmethylated 2'-O RNA.

With this in mind, we generated mutants in SARS-CoV NSP16 that ablated 2'-O-MTase activity by targeting and replacing critical residues within a conserved motif. While the resulting viruses remained replication competent, NSP16 mutants were attenuated in IFN competent cells and had reduced pathogenesis *in vivo*. Additional studies confirmed increased type I IFN sensitivity but failed IFN augmentation or restoration in IFNAR^{-/-} mice. However, deficiency in either MDA5 or IFIT family members resulted in enhanced replication *in vitro* and restored virulence *in vivo*. Finally, targeting the 2'-O-MTase pathway as a live attenuated vaccine platform provided a rational approach for improved prevention of SARS-CoV infection. Overall, the work highlights the importance of 2'-O-MTase activity within the context of SARS-CoV pathogenesis and indicates that both MDA5, a recognition molecule, and the IFIT family play an important role in mediating this attenuation with restored virulence observed in their absence. In addition, the attenuation and restoration of SARS-CoV via viral and host mutation provides a precise definition of pathway manipulation and a possible target pathway for future therapeutic treatments.

MATERIALS AND METHODS

Viruses, cells, *in vitro* infection, and plaque assays. Wild-type and mutant SARS-CoVs were cultured on Vero E6 cells, grown in Dulbecco modified Eagle medium (DMEM; Gibco, CA), and 5% fetal clone serum (HyClone, South Logan, UT), along with antibiotic/antimycotic (Gibco, Carlsbad, CA). Growth curves in Vero, Calu-3 2B4, and human airway epithelial (HAE) cells were determined as previously described (9, 31). Briefly, cells were washed with phosphate-buffered saline (PBS) and inoculated with virus or mock diluted in PBS for 40 min at 37°C. After inoculation, the cells were washed three times, and fresh medium was added to signify time zero. Samples were harvested at described time point. For IFN pretreatments, 100 U of recombinant human IFN-β (PBL Laboratories)/ml was added to Calu3 cells 16 h prior to inoculation and infected as described above. All virus cultivation was performed in a BSL3 laboratory with redundant fans in biosafety cabinets as described previously by our group (32, 33). All personnel wore powdered air purifying

respirators (3M Breathe Easy) with Tyvek suits, aprons, and booties and were double gloved.

Construction of NSP16 mutant viruses. Both wild-type and mutant viruses were derived from either SARS-CoV Urbani or corresponding mouse-adapted (MA15, referred to here as wild type [WT]) infectious clone as previously described (33, 34). For NSP16 mutant construction, the SARS E fragment (residues 18934 to 24057 of the SARS Urbani genome) cloned within the pSMART vector (Lucigen) was used for alanine scanning mutagenesis of conserved residues in nsp16. For the K46A mutation, two PCR products were generated by using the primers SARS 35 (5'-TGTTGCATTGAGCTTTGGGC-3'; residues 19707 to 19727) and NSP16A- (5'-TGAGTATACGCTGCGACATTCATCATTATCC-3'; residues 20704 to 20734) or the primers NSP16A+ (5'-GTCGACCGTATACTCAACTGTGTCAATAC-3'; residues 20716 to 20748) and 10AgeI- (5'-CATCAAGCGAAAAGGCATCAG-3'; residues 21986 to 22006). The two products were gel purified and joined in an overlapping PCR using primers SARS 36 (5'-TGGAGATTCAGTCATGGAC-3'; residues 20261 to 20280) and 9AgeI- (5'-GTTGAGTGTAATTAGGAGCTTG-3'; residues 21568 to 21589). The resultant product was digested with BbsI and ligated into the SARS E plasmid. For the K170A mutation, fragments were amplified with the primers SARS 35 and NSP16B- (5'-GCTCTGTTATCGCTACAGCTATAGAACCACCCAG-3'; residues 21076 to 21109) or with primers NSP16B+ (5'-AGCTGTAGCGATAACAGACGATTCTTGAATGC-3'; residues 21090 to 21121) and 10AgeI-. These two products were subsequently joined in an overlap PCR using the SARS 36 and 9AgeI- primers. The resulting product was digested with BbsI and inserted into the SARS E plasmid. For the D130A change, a product was generated by PCR using primers NSP16C+ (5'-AAATGGGACCTTATTATAGCGCGATGTATGACC-3'; residues 20956 to 20989) and 10AgeI-. This amplicon was digested with PpuMI and AgeI and then ligated into the SARS E plasmid, which had been similarly digested. Thereafter, plasmids containing wild-type and mutant SARS-CoV genome fragments were amplified, excised, ligated, and purified. *In vitro* transcription reactions were then performed to synthesize full-length genomic RNA, which was transfected into Vero E6 cells. The media from transfected cells were harvested and served as seed stocks for subsequent experiments. Viral mutants were confirmed by sequence analysis prior to use. Synthetic construction of mutants of NSP16 were approved by the University of North Carolina Institutional Biosafety Committee.

RNA isolation, microarray processing, and identification of differential expression. RNA isolation and microarray processing from Calu-3 cells was carried out as previously described (35). Differential expression (DE) for *IFNβ1*, *IFIT1*, *IFIT2*, and *MDA5* was determined by comparing virus-infected replicates to time-matched mock replicates. The criteria for DE were an absolute log₂-fold change of >1.5 and a false discovery rate-adjusted *P* value of <0.05 for a given time point.

Construction of stable-shRNA cell lines. Plasmids containing both green fluorescent protein (GFP) and shRNA targeting IFIT1 or IFIT2 were a gift from Michael Diamond (Washington University). Plasmids were amplified and transfected into Vero E6 cells by using Lipofectamine 2000 (Invitrogen) according to the kit protocols. After transfection, cells underwent puromycin selection for 1 week and were analyzed for GFP expression, with >90% of the cells appearing GFP positive. Cells were then IFN treated and infected as described above.

Ethics statement. The present study was carried out in accordance with the recommendations for care and use of animals by the Office of Laboratory Animal Welfare, National Institutes of Health. The Institutional Animal Care and Use Committee (IACUC) of The University of North Carolina at Chapel Hill (UNC; permit A-3410-01) approved the animal study protocol (IACUC 13-033) followed here.

Mouse infections and vaccinations. Ten-week-old BALB/c or C57BL/6 mice were anesthetized with ketamine and xylazine (in accordance with IACUC/UNC guidelines) and intranasally inoculated with a 50-μl volume containing 10⁵ PFU of SARS-CoV WT virus or SARS-CoV dNSP16 virus or PBS mock infected as indicated in the figure legends.

Infected animals were monitored for weight loss, morbidity, clinical signs of disease, and lung titers were determined as described previously (36). For vaccination experiments, 10-week-old BALB/c mice were infected with 10^2 PFU of dNSP16 as described above, monitored for clinical symptoms for 7 days, and then challenged at 4 weeks postvaccination with 10^5 PFU of SARS-CoV MA15. Female BALB/c mice were purchased from Harlan Labs; IFIT1^{-/-} and MDA5^{-/-} mice, previously described (26, 37), were obtained from Michael Diamond and Marco Colonna (Washington University, St. Louis, MO), bred in-house, and both male and female mice were used for studies; male and female control C57BL/6J and IFNAR^{-/-} mice were obtained from The Jackson Laboratory (Bar Harbor, ME) and an equivalent male/female ratio used for the IFIT1^{-/-}, MDA5^{-/-} and C57BL/6J infection groups. Animal housing, care, and experimental protocols were in accordance with UNC IACUC guidelines.

Whole-body plethysmography. Unrestrained whole-body plethysmography was completed using individual plethysmography chambers (Buxco Research Systems, Wilmington, NC) as previously described (38, 39). Briefly, infected or mock treated animals are introduced to a plethysmography chamber located within a biosafety cabinet in a BSL3 laboratory and allowed to acclimate for 30 min. After acclimation, breathing parameters were measured for a 5-min period. Animals were then returned to their cages and monitored as described above. Animals were introduced into the chamber once per day, with their first introduction into the plethysmography chamber immediately prior to infection, and thereafter at indicated time points postinfection. Animals were randomly assigned to a given chamber each day. Generated data were analyzed via Finepoint software (Buxco Research Systems). Whole-body plethysmography protocols were carried out in accordance with UNC IACUC guidelines.

Histological analysis of infected mice. Lung tissues for histological analysis were prepared as described previously (40). Briefly, lung tissue was fixed in 10% formalin (Fisher) for at least 7 days, tissues were embedded in paraffin, and 5- μ m sections were prepared by the UNC histopathology core facility. To determine the extent of inflammation, sections were stained with hematoxylin and eosin (H&E) and scored in a blinded manner. Scoring evaluated pathological changes in the airways (apoptosis, denuded airway epithelial cells, debris, inflammation [scored from 0 to 3]), vasculature (perivascular cuffing [scored from 0 to 3]), and the parenchyma (hyaline membranes, inflammation, and edema [scored from 0 to 3]). Images were captured using an Olympus BX41 microscope with an Olympus DP71 camera.

Meta-analysis of WT SARS-CoV infection. *In vitro* and *in vivo* RNA expression and proteomics data were derived from previous studies with SARS-CoV (31, 40). The raw microarray data are accessible through the NCBI Gene Expression Omnibus (GEO) (41) through GEO series accession numbers GSE33267 and GSE33266. Raw proteomics data corresponding to peptide identifications used to populate the AMT tag database are available at the PRoteomics IDentification (PRIDE) database (<http://www.ebi.ac.uk/pride/>) under the project name "A Systems Biology Approach to Emerging Respiratory Viral Diseases" in the PRIDE Public Projects folder and corresponding to PRIDE accession numbers 19855 to 19860 and 19877 to 19890. The raw quantitative proteomics data can be accessed at the Pacific Northwest National Laboratory's Biological Mass Spectrometry Data and Software Distribution Center (<http://omics.pnl.gov/>) in the systems virology contract data folder within the browse available data folder. All data sets and associated metadata have been submitted to Virus Pathogen Resource (<http://www.viprbrc.org>). Additional details from the present study and similar studies can be accessed through the Systems Virology website (<http://www.systemsvirology.org>).

RESULTS

CoV NSP16 are members of the S-SAM-dependent 2'-O-MTase family (20); although they share little sequence identity, each member maintains a KDKE catalytic tetrad required for activity (Fig. 1A). Mutation at any one of these residues ablates 2'-O-

MTase function (21). In addition, NSP16, unlike other 2'-O-MTases, also requires a stimulatory subunit, NSP10 (20). Targeting either its catalytic subunit or the interaction with NSP10 provides a means to ablate 2'-O methylation of CoV mRNA and evaluate NSP16's impact on pathogenesis (Fig. 1A). In the present study, we focused on the catalytic tetrad. Using the SARS-CoV Urbani infectious clone (33), we generated three mutant viruses with individual alanine substitution within the NSP16 tetrad (K46A, K170A, and D130A [Fig. 1A, inset]), shown to ablate 2'-O-MTase function *in vitro* biochemical assays for coronaviruses (25). Each virus was viable and grew to robust titers in Vero cells following a low-multiplicity infection (Fig. 1B). However, all three mutants were attenuated after infection of IFN competent Calu3 respiratory cells; endpoint titers revealed an approximately 10- to 500-fold reduction in log endpoint titers 48 h postinfection (hpi), depending on the mutant (Fig. 1C). With future *in vivo* experiments in mind, we constructed a mouse-adapted mutant NSP16 virus based on the D130A mutation. This mutation had maintained the most robust replication in Calu3 cells, required no additional passages to generate robust stock titers, and corresponded to a previously generated mutant in related mouse hepatitis virus (26). The resulting mouse-adapted NSP16 mutant virus (dNSP16) also maintained equivalent replication in Vero cells relative to wild-type mouse-adapted SARS-CoV (MA15; referred to here as WT [data not shown]), and both were used for the remainder of the experiments.

NSP16 mutant viruses are attenuated at late time points in respiratory cells and *in vivo*. Using the mouse-adapted D130A mutant (dNSP16), we evaluated its ability to replicate in immunocompetent respiratory cells without its 2'-O-MTase activity. In Calu3 cells, dNSP16 viruses maintains similar replication kinetics to WT SARS-CoV over the first 24 hpi; however, at late time points (48 and 72 hpi), an \sim 10-fold attenuation was noted in dNSP16 infection, which is consistent with the Urbani mutant NSP16 viruses (Fig. 2A). Similarly, primary human airway epithelial (HAE) cultures also maintained a 5- to 10-fold reduction in titer at a later time point, indicating attenuation in cells typically targeted by SARS-CoV in humans (Fig. 2B). Together, the data indicated that the absence of 2'-O-MTase activity has an impact during a low-multiplicity infection of immunocompetent respiratory cells.

Initial *in vivo* studies in 10-week-old BALB/c mice also revealed marked attenuation of dNSP16 compared to WT SARS-CoV. At early time points, dNSP16-infected mice maintained equivalent levels of weight loss to WT-infected animals (Fig. 2C). However, as the infection progressed, dNSP16-infected mice begin to recover weight and have increased survival compared to WT-infected mice (Fig. 2C and data not shown). Similarly, although virus titers in the lung remain equivalent at day 2 postinfection, a nearly 1,000-fold decrease in dNSP16 virus titer is observed at 4 days postinfection (dpi) (Fig. 2D). Examination of lung function also revealed a significant attenuation in dNSP16-infected mice. Both measured airway resistance (penH) and expiratory flow rates (EF50) showed only minimal signs of disease after infection with the dNSP16 mutant (Fig. 2E and F). In contrast, after WT infection airway resistance and expiratory flow difficulties peaked at days 2 and 4, respectively, a finding consistent with previous studies (V. D. Menachery et al., unpublished data). Together, the data indicated a robust attenuation of SARS-CoV mutant lacking 2'-O-MTase activity in a variety of pathogenic outcomes.

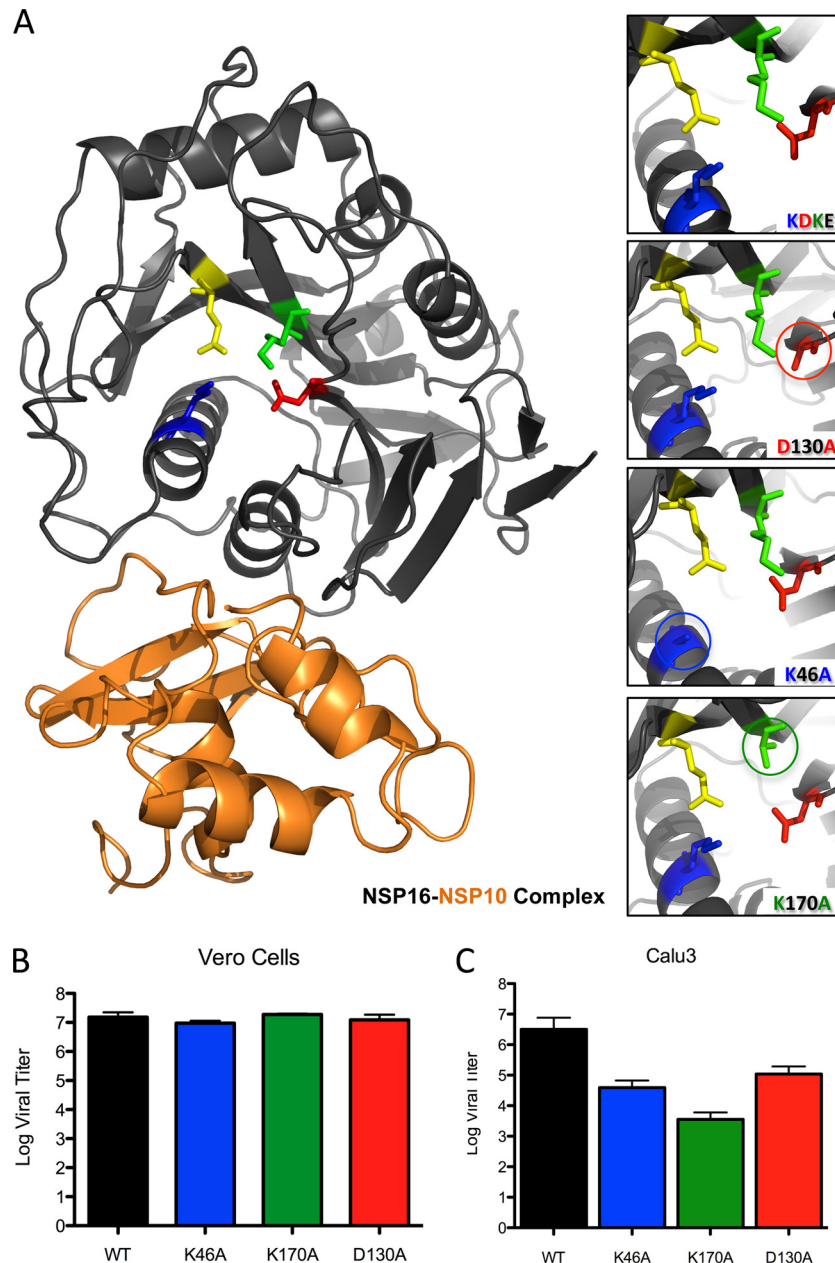


FIG 1 Construction of SARS-CoV NSP16 mutant viruses. (A) SARS-CoV NSP16 protein (black) bound to NSP10 (orange) based on published crystal structure (21). The individual residues of the conserved KDE motif required for MTase function are highlighted in complex, and the insets (on the right side) demonstrate wild-type and constructed NSP16 mutants with alanine substitution at circled residues. (B and C) Endpoint virus titers of wild-type icSARS-CoV and icSARS NSP16 mutants in Vero cells (multiplicity of infection [MOI] = 0.01) (B) and Calu3 airway epithelial cells (MOI = 0.01) (C).

dNSP16 mutant viruses are sensitive to type I IFN but not completely restored by its absence *in vivo*. Attenuation at late time points after both low-multiplicity infection and *in vivo* is possibly indicative of sensitivity to bystander/feedback IFN signaling. Coupled with minimal attenuation in Vero cells, which lack IFN production (42), the data suggested that dNSP16 mutants were sensitive to the type I IFN response. To test this idea, Vero cells were pretreated with 100 U of IFN- β /ml 16 h prior to infection with either dNSP16 or WT SARS-CoV. After a high-multiplicity infection, IFN treatment had little to no impact on WT SARS-CoV replication; in contrast, IFN pretreatment resulted in

the substantial attenuation of dNSP16 with a nearly 10,000-fold reduction in virus titer 24 hpi compared to untreated cells (Fig. 3A). Together, the results confirm that IFN resistance demonstrated by WT SARS-CoV requires the continued maintenance of the 2'-O-MTase activity of NSP16.

Having demonstrated increased sensitivity of dNSP16 to type I IFN, we next sought to determine whether an increased IFN response played a significant role in mutant virus attenuation. After infection with either WT SARS-CoV or dNSP16, Calu3 cells showed no augmentation or changes in underlying kinetics of the type I IFN response (Fig. 3B). Examining the expression of *IFNB1*

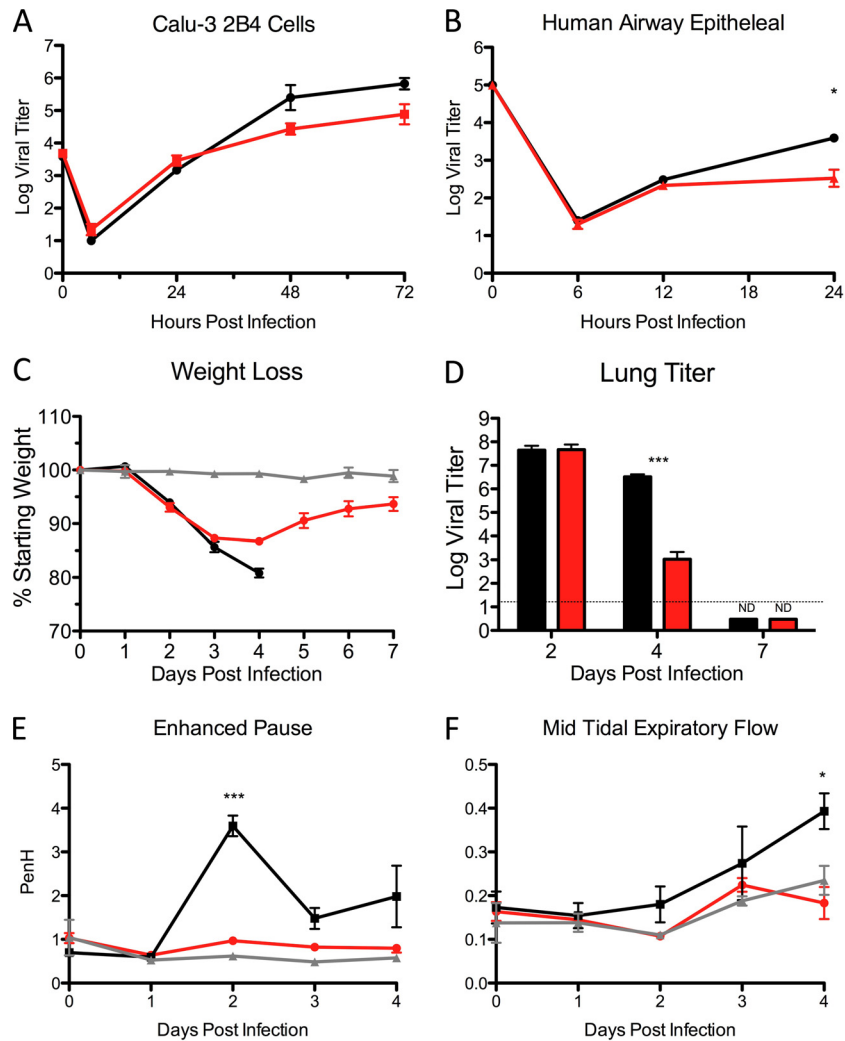


FIG 2 dNSP16 mutant viruses attenuation *in vitro* and *in vivo*. (A and B) Virus titers after infection of Calu3 cells (A) or human airway epithelial (HAE) cells (B) with SARS-CoV WT or dNSP16 at an MOI of 0.01. Time zero represents input titers. (C to F) Weight loss ($n > 5$ for WT and dNSP16 groups) (C), lung virus titer ($n = 3$ per group) (D), airway resistance (E), and expiratory flow (F) after infection of female BALB/c mice with 10^5 PFU of SARS-CoV WT or dNSP16. *P* values based on the Student *t* test are marked (*, $P < 0.05$; ***, $P < 0.001$).

indicated that both WT and dNSP16 infections had delayed (>12 hpi), but nevertheless substantial induction of type I IFN transcripts at late times. Similarly, C57BL/6 mice infected with WT or mutant saw no change in *IFNB1*, as measured by microarray analysis (Fig. 3C). Similar results were observed for both *IFNA4* and *IFNL1* both *in vitro* and *in vivo* (data not shown). In addition, infection of mice lacking type I IFN receptor (*IFNAR*^{-/-}) also suggested that IFN played an important, but limited role in dNSP16 attenuation. After infection, dNSP16-infected *IFNAR*^{-/-} mice maintained slightly augmented virus titers compared to WT SARS-CoV at 2 dpi. By day 4, dNSP16 demonstrated a smaller, but significant 10-fold reduction in lung titer compared to WT (Fig. 3D). Relative to the deficit observed in wild-type mice (Fig. 2D), this represented a nearly 100-fold augmentation of viral replication. However, partial restoration of viral replication in *IFNAR*^{-/-} mice failed to impact pathogenesis since the weight loss data indicated continued attenuation of dNSP16 (Fig. 3E). Together, the data showed that type I IFN plays a significant role in

replication deficits of dNSP16, but additional factors contribute to attenuation independent of downstream type I IFN signaling.

IFIT and MDA5 deficiency restores SARS-CoV dNSP16 mutant. Having demonstrated that type I IFN deficiency alone was insufficient to restore virulence to dNSP16 mutant SARS-CoV, we next sought to determine whether IFN augmented, but independent antiviral genes play a prominent role. Recent works had identified 2'-O methylation as a critical distinction between self and nonself RNA. Therefore, we chose to focus on host antiviral proteins that had previously been shown to target RNA species lacking 2'-O methylation and are IFN independent: MDA5 and the IFIT family of proteins (12, 26). Notably, both IFIT1 and MDA5 had been previously been shown by our group to be induced even in the absence of type I IFN receptor during SARS-CoV infection (43). Using a comprehensive systems biology approach with RNA ($>20,000$ transcripts) and proteomic data ($>2,000$ proteins) (31), MDA5, IFIT1, and IFIT2 expression were examined following WT SARS-CoV infection of Calu3 cells (Fig. 4A to C). The results

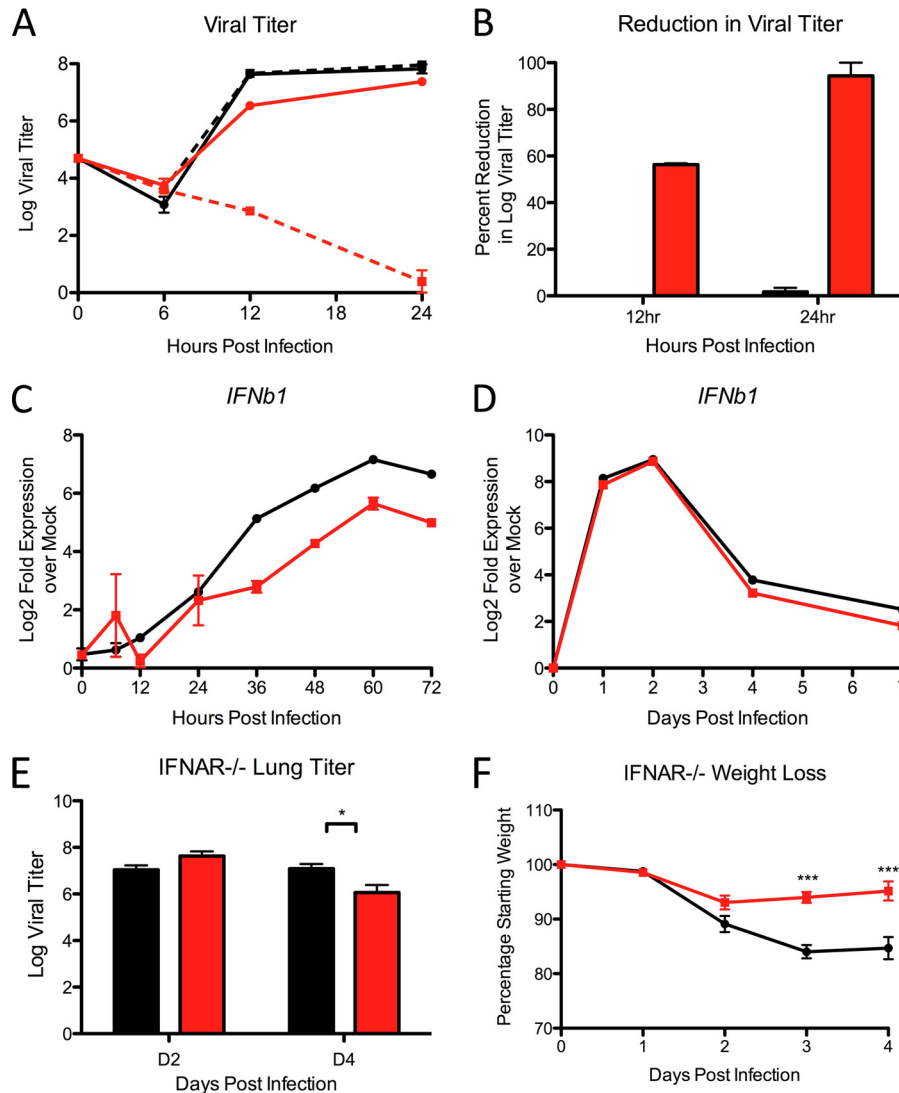


FIG 3 dNSP16 is more sensitive to IFN but is not restored by type I IFN deficiency. (A) Mock-treated (solid lines) or IFN- β pretreated (dotted lines) Vero cells infected with either SARS-CoV WT (black) or dNSP16 (red) at an MOI of 5. (B) Percentage reduction in log virus titer derived from panel A for WT (black) or dNSP16 (red). (C and D) RNA expression of *IFNb1* from Calu3 cells (C) or C57BL/6 (D) mice after infection with WT or dNSP16 SARS-CoV. (E and F) Viral lung titers ($n > 3$ per group) (E) and weight loss ($n > 6$ per group) (F) after infection of female, 10-week-old IFNAR^{-/-} mice with SARS-CoV WT (black) or dNSP16 (red). *P* values based on the Student *t* test are marked (*, $P < 0.05$; ***, $P < 0.001$).

indicated that both MDA5 and IFIT family members were induced at the RNA and protein levels. In addition, when the proteomic values are overlaid with replication during low-multiplicity infection (Fig. 2A), the kinetics of MDA5 and IFIT protein production corresponded with the kinetics of dNSP16 attenuation. Similarly, *in vivo* proteomics data show that both RNA induction and protein production of MDA5, IFIT1, and IFIT2 peak at 4 dpi, which also corresponds to *in vivo* attenuation of dNSP16 (Fig. 4D to F) (40). However, *in vitro* studies directly comparing WT and dNSP16 revealed neither earlier induction nor augmented expression of IFIT1, IFIT2, or MDA5 after the mutant infection (Fig. 5A to C). Similarly, C57BL/6 mice infected with either WT or dNSP16 showed no distinction in the magnitude or kinetics of expression (Fig. 5D to F). These results suggested that the deficit in dNSP16 derives from the IFIT effector function rather than augmented sensing and signaling provided by MDA5

(44, 45). To confirm the effector role of IFIT1 and IFIT2, we observed dNSP16 replication in their absence. GFP-expressing shRNA constructs were used to develop stable IFIT1, IFIT2, and MDA5 knockdown (KD) Vero cell lines under puromycin selection. After IFN pretreatment, both IFIT1 and IFIT2 KD cells infected with WT SARS-CoV exhibited a modest increase in viral replication at 24 hpi (Fig. 5G); by 48 hpi, WT virus titers are equivalent in control and KD cell lines, likely due to NSP16 activity. In contrast, dNSP16 infection resulted in a substantial increase in viral replication in both IFIT1 and IFIT2 KD cell lines pretreated with IFN (Fig. 5H). In addition, MDA5 KD cells demonstrated no measurable change in WT or dNSP16 replication (data not shown). Together, these results suggested that IFN-dependent attenuation of dNSP16 is strongly, but not completely dependent on the individual effector activities of IFIT1 and IFIT2.

Having established an effector role for the IFIT family in

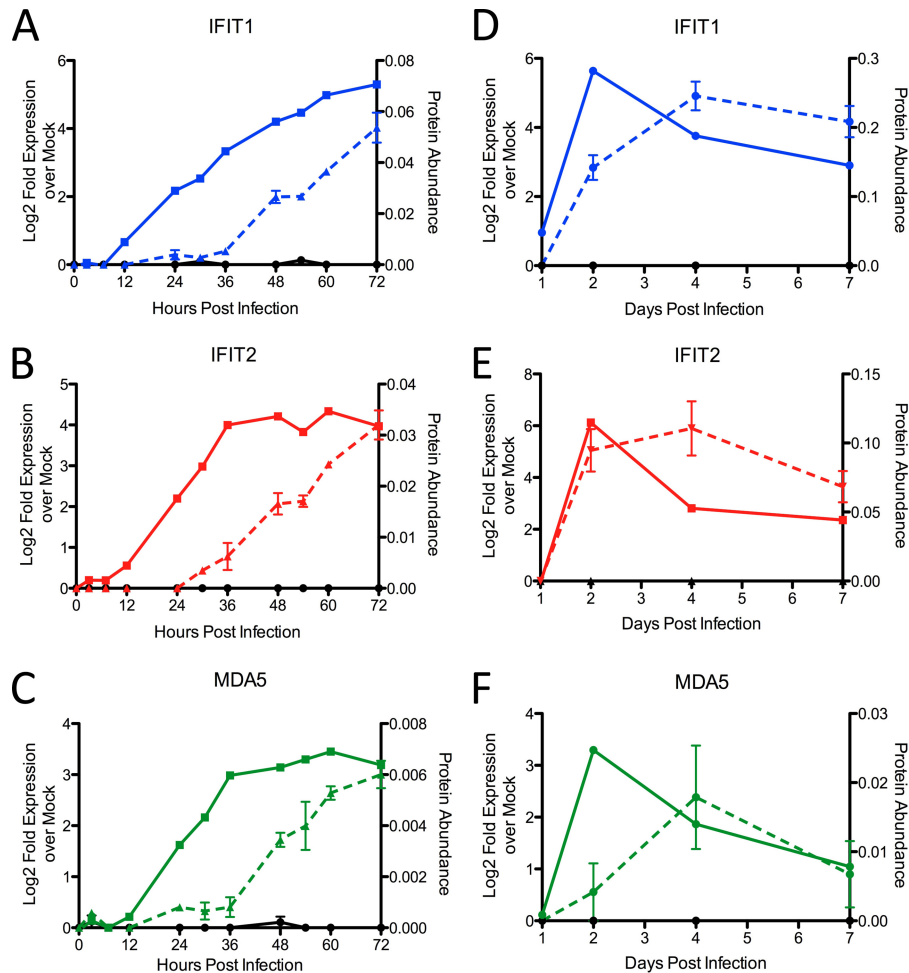


FIG 4 Kinetic expression of MDA5 and IFIT proteins correspond to dNSP16 attenuation. (A to C) RNA (solid line) and protein (dashed line) expression of IFIT1 (A), IFIT2 (B), and MDA5 (C) in Calu3 cells after infection with WT icSARS-CoV. (D to F) RNA (solid) and protein (dashed) expression of IFIT1 (D), IFIT2 (E), and MDA5 (F) after infection of C57BL/6 mice.

dNSP16 attenuation *in vitro*, we next sought to examine the role of IFIT1, as well as the sensor molecule MDA5, *in vivo*. Male and female 10-week-old WT, MDA5^{-/-}, and IFIT1^{-/-} C57BL/6 mice were infected with either dNSP16 or WT and monitored over a 7-day time course. C57BL/6 mice maintained attenuation of dNSP16 relative to WT in terms of weight loss and viral replication confirming BALB/c results (Fig. 6A). In contrast, both MDA5^{-/-} and IFIT1^{-/-} mice resulted in restored virulence for dNSP16. In the absence of MDA5 or IFIT1, dNSP16 caused similar weight loss as WT in both mouse lines (Fig. 6B and C). Similarly, the absence of either of these proteins resulted in D4 virus titers equal to or greater than WT titers in WT mice (Fig. 6D). Although the absence of MDA5 and IFIT1 enhanced WT replication at day 4, no concurrent change in weight loss was observed. This result suggested that MDA5 and IFIT1 still impacted WT SARS-CoV replication but did not alter pathogenesis. Notably, the absence of either IFIT1 or MDA5 restored the ability of dNSP16 to cause breathing difficulties. Changes in airway resistance (penH) and expiratory flow rate (EF50) after dNSP16 infection overlapped changes observed during WT infection (Fig. 6E to G). In addition, lung sections revealed that attenuation of dNSP16 in C57BL/6 was reversed in both MDA5^{-/-} and IFIT1^{-/-} mice (Fig. 7). Although

day 2 and day 4 showed only minor changes (data not shown), examination of day 7 histology revealed reduced disease in dNSP16-infected B6 mice relative to WT infection in terms of broad lung disease, edema, and vascular cuffing (Fig. 7A and B). In contrast, both MDA5^{-/-} and IFIT1^{-/-} mice had broad similarities in lung damage between WT and dNSP16 (Fig. 7C to F). In addition, while airway disease remained similar in all groups (data not shown), the dNSP16 attenuation in edema and vasculature disease was absent in IFIT1^{-/-} and MDA5^{-/-}, as measured by histology scoring (Fig. 7G to H). Together, the infection data illustrated that the absence of SARS-CoV 2'-O-MTase was complemented by the absence of either MDA5 or IFIT1, thus restoring pathogenesis to dNSP16 *in vivo*.

Targeting 2'-O-MTase pathways for vaccination. Effective treatments for SARS-CoV and other CoV infection do not currently exist (18, 57). Therefore, studying and targeting 2'-O methylation may provide novel strategies for developing effective treatments to SARS-CoV and potentially global methods to rationally design treatments for other RNA viruses. *In vivo* attenuation raised the possibility of utilizing 2'-O-MTase mutants as a live-attenuated vaccine backbone. This approach permits robust viral replication during early times, but accelerated viral clearance

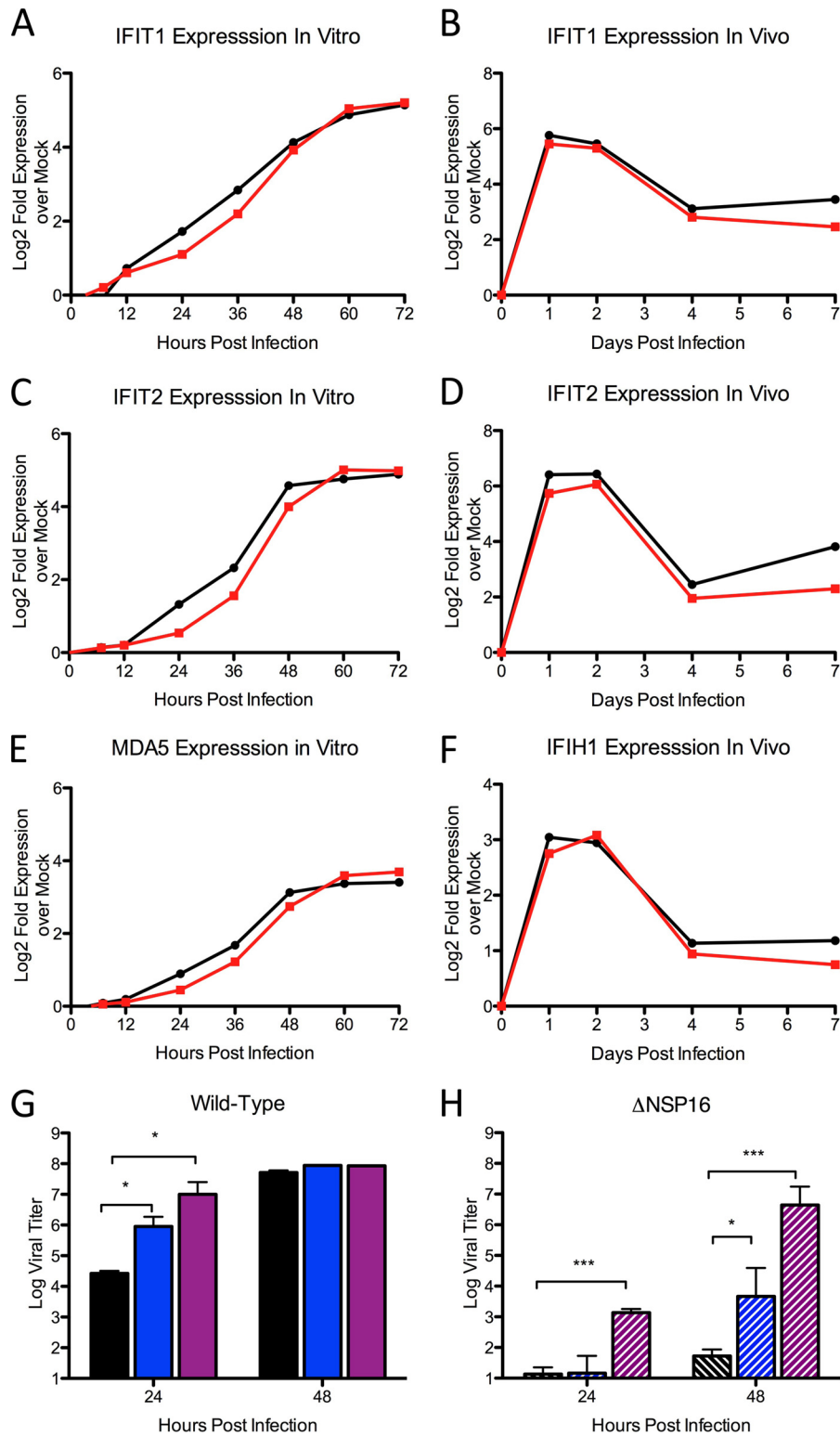


FIG 5 ISG expression kinetics and effector function after *in vitro* infection with dNSP16. (A to C) *In vitro* RNA expression of IFIT1 (A), IFIT2 (B), and MDA5 (C) after infection at an MOI of 5 of Calu3 cells with WT SARS-CoV (black) or dNSP16 (red), as measured by microarray. (D to F) *In vivo* RNA expression of IFIT1 (D), IFIT2 (E), and MDA5 (F) after infection of C57BL/6 mice with WT SARS-CoV (black) or dNSP16 (red). (G to H) Vero cells expressing shRNA targeting IFIT1 (blue), IFIT2 (purple), or no shRNA (black) were pretreated with IFN- β and infected with WT SARS-CoV (G) or dNSP16 (H). *P* values based on Student *t* test and are marked as indicated (*, *P* < 0.05; ***, *P* < 0.001).

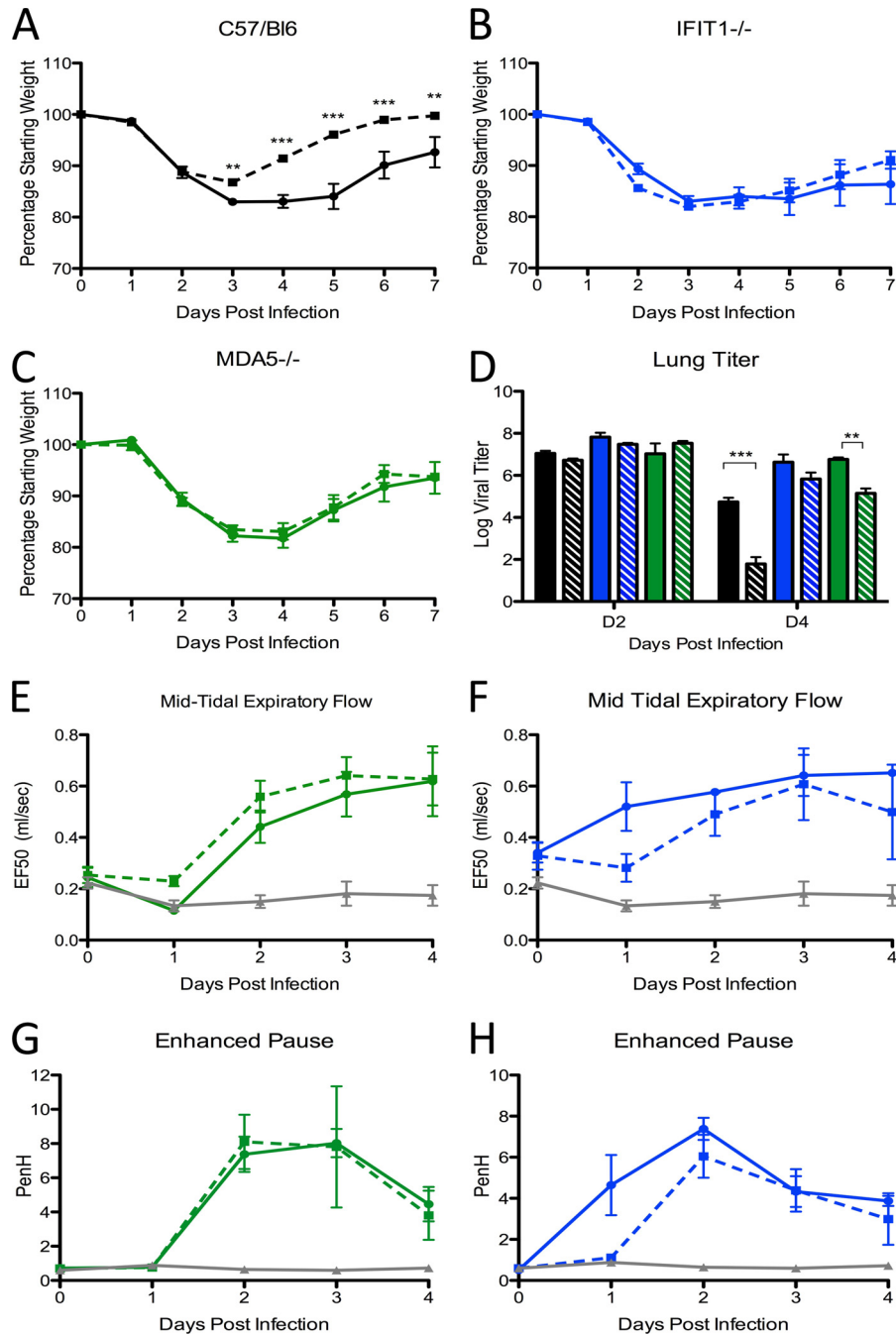


FIG 6 Pathogenesis after infection of MDA5^{-/-} or IFIT1^{-/-} mice with dNSP16. (A to H) Male and female C57BL/6 (black, $n > 13$ per group), MDA5^{-/-} (green, $n > 13$ per group), and IFIT1^{-/-} (blue, $n > 8$ per group) mice were infected with SARS-CoV WT (solid lines) or dNSP16 (dashed line) and monitored for weight loss (A to C), virus titer in the lung (D), expiratory flow (E and F), and airway resistance (G and H). For panels E to H, data from mock-infected IFIT1^{-/-} (two mice) and MDA5^{-/-} (one mouse) animals were combined to provide a relative baseline for respiratory function. P values based on Student t test and are marked as indicated (*, $P < 0.05$; **, $P < 0.01$; ***, $P < 0.001$).

and immune priming at late times postinfection. To evaluate dNSP16 as a possible vaccine, 10-week-old BALB/c mice were vaccinated with 10^2 PFU of dNSP16 or PBS mock infected. Animals were monitored for 7 days and subsequently challenged with a lethal dose (10^5) of SARS-CoV WT at 4 weeks postvaccination. The results demonstrated that dNSP16-infected mice suffered minimal weight loss during initial vacci-

nation (data not shown). Postchallenge with WT, vaccinated mice lost $<5\%$ of body weight and were protected from lethal challenge (Fig. 8A and B). In contrast, mock-vaccinated mice showed significant weight loss, and all mice died by day 4. In addition, serum from vaccinated mice proved to be effective in neutralizing WT control virus with plaque reduction neutralization test 50 (PRNT₅₀) titers exceeding 1/1,600 (Fig. 8C).

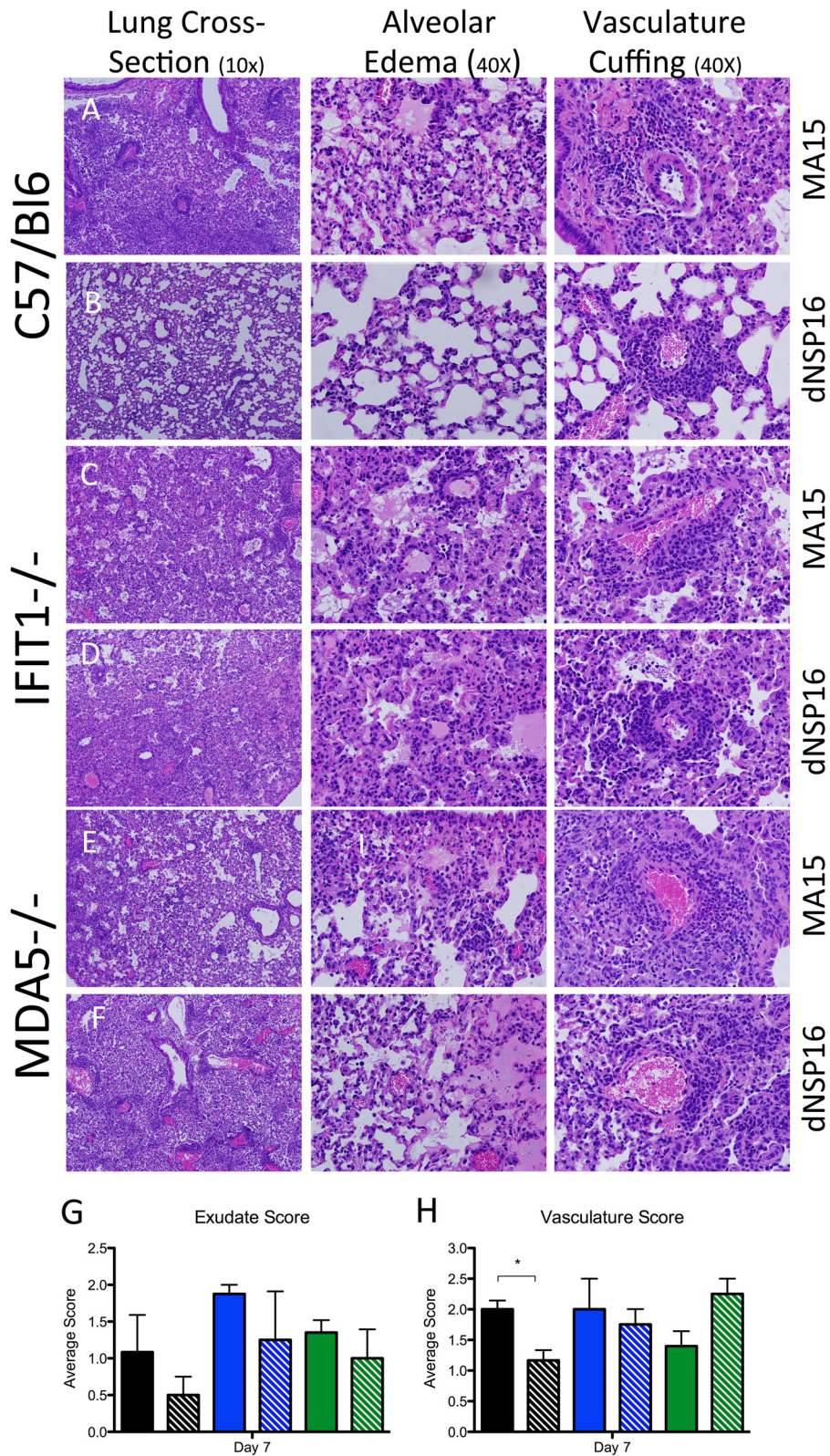


FIG 7 Histological analysis of C57BL/6, IFIT1^{-/-}, and MDA5^{-/-} mice after infection with WT-SARS-CoV and dNSP16. (A to F) Representative images show broad lung cross-sections (first column, 10×), alveolar edema (second column, 40×), and vascular cuffing (third column, 40×) after WT-SARS-CoV (A, C, and E) or dNSP16 (B, D, and F) infection of C57BL/6 (A and B), IFIT1^{-/-} (C and D), and MDA5^{-/-} (E and F) mice. (G and H) Blinded histology scoring of alveolar exudates (G) and vasculature disease (edema and perivascular cuffing) (H) after WT (solid) or dNSP16 (hatched) infection of C57BL/6 (black), IFIT1^{-/-} (blue), and MDA5^{-/-} (green) mice 7 days postinfection. *P* values based on Student *t* test and are marked as indicated (*, *P* < 0.05).

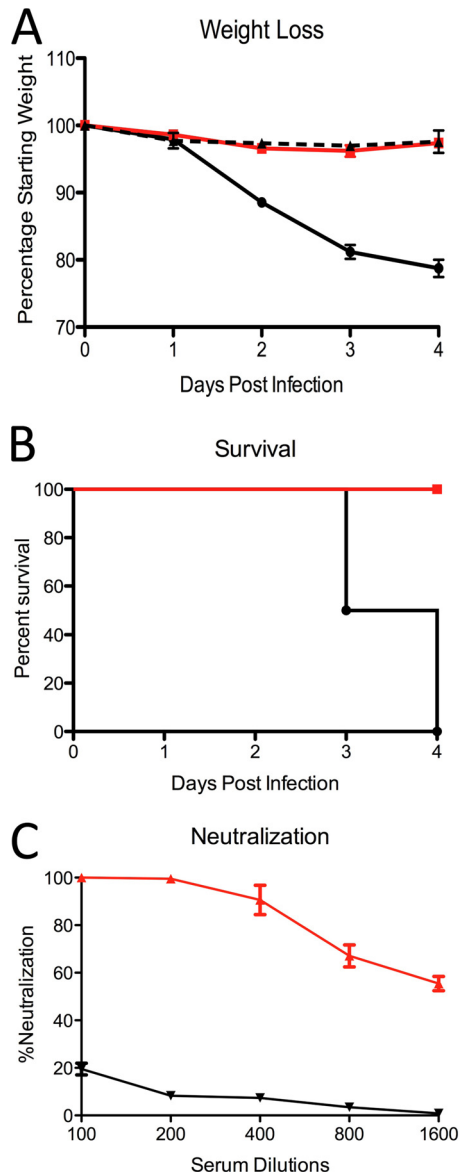


FIG 8 Vaccination with dNSP16 protects from lethal challenge. (A and B) Weight loss (A) and lethality (B) after infection of 10-week-old female BALB/c mice vaccinated with 100 PFU of dNSP16 or PBS ($n = 6$), monitored for 28 days, and then challenged with SARS-CoV WT at 10^5 PFU. (C) Neutralization titer for WT-SARS-CoV from serum of dNSP16-vaccinated mice or mock-vaccinated mice 28 days postinfection. P values are based on the Student t test and are marked as indicated (*, $P < 0.05$; **, $P < 0.01$; ***, $P < 0.001$).

Together, the data demonstrated that targeting viral 2'-O-MTases as a valid strategy for rapid, rational vaccine design.

DISCUSSION

The data in this study illustrate both the importance of 2'-O-MTase activity to SARS-CoV pathogenesis and the immune pathways that target this activity to mediate antiviral defense. While NSP16 activity has only a minimal impact on the underlying viral life cycle of SARS-CoV, its absence resulted in significant attenuation under immune selective pressure. *In vitro*, the lack of 2'-O-MTase activity resulted in a modest, but significant reduction in virus titers at late time points in both an immunocompetent re-

spiratory cell line and primary human airway cultures. Similarly, *in vivo* attenuation was observed in regard to viral replication, weight loss, and breathing functionality following dNSP16 infection. In addition, the absence of NSP16 activity rendered the mutant virus exquisitely sensitive to type I IFN pretreatment. However, despite the enhanced sensitivity, knocking out type I IFN signaling was not sufficient to fully restore virulence to the NSP16 mutant virus *in vivo*. Further analysis revealed MDA5 and the IFIT family members, both of which target unmethylated 2'-O capped RNA, as critical in mediating dNSP16 attenuation. The absence of either MDA5 or IFIT1 *in vivo* resulted in augmented replication, restored weight loss, and reduced breathing functionality replicating phenotypes seen in SARS-CoV WT-infected controls. Together, the data illustrate the attenuation and restoration of SARS-CoV mutant lacking 2'-O-MTase activity and have possible implications for future therapeutic treatments.

The attenuation of SARS-CoV 2'-O-MTase mutants was consistent with reports in other RNA viruses. Both flaviviruses and murine coronaviruses have been generated previously, targeting substitutions with the same KDKE motif utilized in these studies (12, 26, 46, 47). Although these mutant viruses have been shown to be viable without 2'-O-MTase activity, they maintain IFN based attenuation *in vitro* and *in vivo*. Similarly, SARS-CoV dNSP16 had normal replication kinetics and increased sensitivity to type I IFN treatment relative to WT. However, unlike 2'-O-MTase mutants in other coronaviruses (12), dNSP16 failed to induce a more robust type I IFN response. Similarly, while the absence of type I IFN receptor augmented viral replication *in vivo*, it failed to restore virulence to dNSP16, in contrast to previous findings with West Nile virus (26). Together, the results indicated that despite increased IFN sensitivity, dNSP16 maintained the ability to antagonize the type I IFN response equivalently to WT SARS-CoV. In addition, the data indicate that host pathways independent of type I IFN play a substantial role in limiting dNSP16 pathogenesis *in vivo*.

Shifting focus, we next examined MDA5 and IFIT proteins which had previously been shown to play important roles in mediating attenuation of 2'-O-MTase mutants. Both MDA5 and IFIT family members are IFN responsive genes (48) but have been shown to be induced after SARS-CoV infection independent of type I IFN receptor (43). Based on host transcription and protein kinetics following WT SARS infection, both MDA5 and IFIT production corresponded with attenuation of dNSP16 *in vitro* and *in vivo*. Similarly, SARS-CoV dNSP16 virus infection of either IFIT1^{-/-} or MDA5^{-/-} mice resulted in restored virulence in terms of viral replication and weight loss relative to WT. Notably, the results also showed restored pathogenesis in terms of breathing dysfunction in mice and histology scoring. While SARS-CoV dNSP16 infection resulted in minimal breathing changes in wild-type mice, both airway resistance and lung flow rate were reduced after dNSP16 infection with levels equivalent to WT in IFIT1^{-/-} and MDA5^{-/-} mice. These results contrast with findings observed with West Nile virus, dengue virus, and mouse hepatitis virus that, despite augmented viral replication and tissue distribution in IFIT1^{-/-} and MDA5^{-/-} mice, failed to fully restore virulence and pathogenesis to the 2'-O-MTase mutants (12, 26, 46). This contrast within 2'-O-MTase mutants in the same and other viral families suggests that tissue and pathogen specificity may play a significant role in differences in mutant restoration. A previous report has detailed differing requirements for IFIT1 and IFIT2 in

the brain versus peripheral tissues following viral challenge (49). In addition, cell-specific and tissue-specific immune responses vary greatly between the target cells of mouse hepatitis virus (liver cells), flaviviruses (immune cells), and SARS-CoV (lung epithelia), thus altering the necessity and requirements for specific ISGs. Within the lung, it appears that both MDA5 and IFIT family members play critical roles in mediating attenuation of SARS-CoV 2'-O-MTase mutant, and these genes are augmented, but not dependent on type I IFN.

Understanding the attenuation and host-mediated restoration of dNSP16 provides an opportunity to design novel therapeutics that target this pathway for treatment of CoV and other RNA virus infections. Effective treatments and vaccines for SARS-CoV and other CoV infection do not currently exist (18, 57). Both subunit and adjuvanted-killed vaccines have been explored but have been plagued by vaccine failure and/or induced immune pathology, especially in aged animal models (36, 50–52). Two live attenuated vaccine platforms that employ a mutation in ExoN or a deletion in the E protein have been shown to be effective in both young and old mice (52–54). However, recent work suggested that a sufficient level of viral replication is required to initiate robust immunity (52), and both the ExoN and ΔE mutants have significant attenuation of viral replication, even at early time points following infection. In contrast, *in vivo* attenuation of dNSP16 suggested that vaccination with this mutant could maintain robust replication at early time points but would induce rapid, immune-based clearance at late time points. Our results indicated that vaccination of young animals with a low dose of dNSP16 resulted in complete protection from homologous WT SARS-CoV challenge. In young animals, dNSP16-induced neutralization titers exceeded those of most vaccine platforms tested to date, recognizing that direct comparisons are very difficult because of variations in protocols, vaccine doses, age, challenge doses, and other study design conditions (36, 50, 52, 54). While further study is required, especially in more vulnerable aged populations, the present study provides a proof of principle in utilizing 2'-O-MTase mutants as a successful vaccine platform for CoVs and is consistent with a similar approach using the 2'-O-MTase mutant of dengue virus as a successful live-attenuated vaccine (46).

In addition to a vaccine platform, targeting the 2'-O-MTase pathway for drug treatment provides a novel means to treat CoV infection. One approach would directly target the catalytic KDKE domain of the viral MTase blocking its target binding. This approach would result in IFN-based attenuation and possibly prove effective against any virus that uses a virally encoded 2'-O-MTase. A second approach disrupts CoV infection by directly preventing interaction with NSP10, a required component for CoV NSP16 activity (20). For both approaches, target drugs and small peptide inhibitors exist (55, 56), but effective treatment must also overcome type I IFN blockade induced by the virus, thus permitting the production of immune effectors that mediate attenuation. Therefore, drugs targeting this pathway may prove most effective in combination with IFN stimulatory agents.

Overall, we demonstrate here that SARS-CoV viruses that lack 2'-O-MTase activity are viable but attenuated both *in vitro* and *in vivo*. In addition, the results indicate that while attenuation is immune mediated, it is only partially dependent on type I IFN. Further examination confirmed that both MDA5 and IFIT family members were necessary components required to mediate dNSP16 attenuation. In the absence of either MDA5 or IFIT1,

dNSP16 SARS-CoV had fully restored replication and pathogenesis *in vivo*, successfully complementing the deficit in the 2'-O-MTase activity. Together, these findings have significant implications for both the understanding and the treatment of SARS-CoV and future emerging respiratory coronavirus infections, including MERS-CoV infections.

ACKNOWLEDGMENTS

The research reported here was supported by the National Institute of Allergy and Infectious Diseases, National Institutes of Health, under contract HHSN272200800060C and awards U19AI100625, U19AI109680, and F32AI102561.

We thank Michael Diamond and Marco Colonna for providing reagents and mice.

The content of this paper is solely the responsibility of the authors and does not necessarily represent the official views of the National Institutes of Health.

REFERENCES

1. Perlman S. 1998. Pathogenesis of coronavirus-induced infections: review of pathological and immunological aspects. *Adv. Exp. Med. Biol.* **440**:503–513.
2. Greenberg SB. 2007. Rhinovirus and coronavirus infections. *Semin. Respir. Crit. Care Med.* **28**:182–192. <http://dx.doi.org/10.1055/s-2007-976490>.
3. Becker MM, Graham RL, Donaldson EF, Rockx B, Sims AC, Sheahan T, Pickles RJ, Corti D, Johnston RE, Baric RS, Denison MR. 2008. Synthetic recombinant bat SARS-like coronavirus is infectious in cultured cells and in mice. *Proc. Natl. Acad. Sci. U. S. A.* **105**:19944–19949. <http://dx.doi.org/10.1073/pnas.0808116105>.
4. Peiris JS, Guan Y, Yuen KY. 2004. Severe acute respiratory syndrome. *Nat. Med.* **10**:S88–S97. <http://dx.doi.org/10.1038/nm1143>.
5. Muradrasoli S, Balint A, Wahlgren J, Waldenstrom J, Belak S, Blomberg J, Olsen B. 2010. Prevalence and phylogeny of coronaviruses in wild birds from the Bering Strait area (Beringia). *PLoS One* **5**:e13640. <http://dx.doi.org/10.1371/journal.pone.0013640>.
6. Donaldson EF, Haskew AN, Gates JE, Huynh J, Moore CJ, Frieman MB. 2010. Metagenomic analysis of the viromes of three North American bat species: viral diversity among different bat species that share a common habitat. *J. Virol.* **84**:13004–13018. <http://dx.doi.org/10.1128/JVI.01255-10>.
7. Rihtaric D, Hostnik P, Steyer A, Grom J, Toplak I. 2010. Identification of SARS-like coronaviruses in horseshoe bats (*Rhinolophus hipposideros*) in Slovenia. *Arch. Virol.* **155**:507–514. <http://dx.doi.org/10.1007/s00705-010-0612-5>.
8. Dominguez SR, O'Shea TJ, Oko LM, Holmes KV. 2007. Detection of group 1 coronaviruses in bats in North America. *Emerg. Infect. Dis.* **13**:1295–1300. <http://dx.doi.org/10.3201/eid1309.070491>.
9. Josset L, Menachery VD, Gralinski LE, Agnihotram S, Sova P, Carter VS, Yount BL, Graham RL, Baric RS, Katze MG. 2013. Cell host response to infection with novel human coronavirus EMC predicts potential antivirals and important differences with SARS coronavirus. *mBio* **4**:e00165–00113. <http://dx.doi.org/10.1128/mBio.00165-13>.
10. Corman VM, Eckerle I, Bleicker T, Zaki A, Landt O, Eschbach-Bludau M, van Boheemen S, Gopal R, Ballhaus M, Bestebroer TM, Muth D, Muller MA, Drexler JF, Zambon M, Osterhaus AD, Fouchier RM, Drosten C. 2012. Detection of a novel human coronavirus by real-time reverse-transcription polymerase chain reaction. *Euro Surveill.* **17**(39):pii20285. <http://www.eurosurveillance.org/ViewArticle.aspx?ArticleId=20285>.
11. Liu L, Dong H, Chen H, Zhang J, Ling H, Li Z, Shi PY, Li H. 2010. Flavivirus RNA cap methyltransferase: structure, function, and inhibition. *Front. Biol.* **5**:286–303. <http://dx.doi.org/10.1007/s11515-010-0660-y>.
12. Züst R, Cervantes-Barragan L, Habjan M, Maier R, Neuman BW, Ziebuhr J, Szretter KJ, Baker SC, Barchet W, Diamond MS, Siddell SG, Ludewig B, Thiel V. 2011. Ribose 2'-O-methylation provides a molecular signature for the distinction of self and non-self mRNA dependent on the RNA sensor Mda5. *Nat. Immunol.* **12**:137–143. <http://dx.doi.org/10.1038/nrm3071>.
13. Weber F, Haller O, Kochs G. 1996. Nucleoprotein viral RNA and mRNA

- of Thogoto virus: a novel "cap-stealing" mechanism in tick-borne orthomyxoviruses? *J. Virol.* 70:8361–8367.
14. Ogino T, Banerjee AK. 2011. An unconventional pathway of mRNA cap formation by vesiculoviruses. *Virus Res.* 162:100–109. <http://dx.doi.org/10.1016/j.virusres.2011.09.012>.
 15. Vasiljeva L, Merits A, Auvinen P, Kaariainen L. 2000. Identification of a novel function of the alphavirus capping apparatus. RNA 5'-triphosphatase activity of Nsp2. *J. Biol. Chem.* 275:17281–17287.
 16. Decroly E, Ferron F, Lescar J, Canard B. 2012. Conventional and unconventional mechanisms for capping viral mRNA. *Nat. Rev. Microbiol.* 10:51–65.
 17. Ivanov KA, Ziebuhr J. 2004. Human coronavirus 229E nonstructural protein 13: characterization of duplex-unwinding, nucleoside triphosphatase, and RNA 5'-triphosphatase activities. *J. Virol.* 78:7833–7838. <http://dx.doi.org/10.1128/JVI.78.14.7833-7838.2004>.
 18. Ivanov KA, Thiel V, Dobbe JC, van der Meer Y, Snijder EJ, Ziebuhr J. 2004. Multiple enzymatic activities associated with severe acute respiratory syndrome coronavirus helicase. *J. Virol.* 78:5619–5632. <http://dx.doi.org/10.1128/JVI.78.11.5619-5632.2004>.
 19. Chen Y, Cai H, Pan J, Xiang N, Tien P, Ahola T, Guo D. 2009. Functional screen reveals SARS coronavirus nonstructural protein nsp14 as a novel cap N7 methyltransferase. *Proc. Natl. Acad. Sci. U. S. A.* 106:3484–3489. <http://dx.doi.org/10.1073/pnas.0808790106>.
 20. Chen Y, Su C, Ke M, Jin X, Xu L, Zhang Z, Wu A, Sun Y, Yang Z, Tien P, Ahola T, Liang Y, Liu X, Guo D. 2011. Biochemical and structural insights into the mechanisms of SARS coronavirus RNA ribose 2'-O-methylation by nsp16/nsp10 protein complex. *PLoS Pathog.* 7:e1002294. <http://dx.doi.org/10.1371/journal.ppat.1002294>.
 21. Decroly E, Debarnot C, Ferron F, Bouvet M, Coutard B, Imbert I, Gluais L, Papageorgiou N, Sharff A, Bricogne G, Ortiz-Lombardia M, Lescar J, Canard B. 2011. Crystal structure and functional analysis of the SARS-coronavirus RNA cap 2'-O-methyltransferase nsp10/nsp16 complex. *PLoS Pathog.* 7:e1002059. <http://dx.doi.org/10.1371/journal.ppat.1002059>.
 22. Debarnot C, Imbert I, Ferron F, Gluais L, Varlet I, Papageorgiou N, Bouvet M, Lescar J, Decroly E, Canard B. 2011. Crystallization and diffraction analysis of the SARS coronavirus nsp10-nsp16 complex. *Acta Crystallogr. Sect. F Struct. Biol. Crystallogr. Commun.* 67:404–408. <http://dx.doi.org/10.1107/S1744309111002867>.
 23. Lugari A, Betzi S, Decroly E, Bonnaud E, Hermant A, Guillemot JC, Debarnot C, Borg JP, Bouvet M, Canard B, Morelli X, Lecine P. 2010. Molecular mapping of the RNA Cap 2'-O-methyltransferase activation interface between severe acute respiratory syndrome coronavirus nsp10 and nsp16. *J. Biol. Chem.* 285:33230–33241. <http://dx.doi.org/10.1074/jbc.M110.120014>.
 24. Bouvet M, Debarnot C, Imbert I, Selisko B, Snijder EJ, Canard B, Decroly E. 2010. In vitro reconstitution of SARS-coronavirus mRNA cap methylation. *PLoS Pathog.* 6:e1000863. <http://dx.doi.org/10.1371/journal.ppat.1000863>.
 25. Decroly E, Imbert I, Coutard B, Bouvet M, Selisko B, Alvarez K, Gorbalenya AE, Snijder EJ, Canard B. 2008. Coronavirus nonstructural protein 16 is a cap-0 binding enzyme possessing (nucleoside-2'-O)-methyltransferase activity. *J. Virol.* 82:8071–8084. <http://dx.doi.org/10.1128/JVI.00407-08>.
 26. Daffis S, Szretter KJ, Schriewer J, Li J, Youn S, Errett J, Lin TY, Schneller S, Züst R, Dong H, Thiel V, Sen GC, Fensterl V, Klimstra WB, Pierson TC, Buller RM, Gale M, Jr, Shi PY, Diamond MS. 2010. 2'-O methylation of the viral mRNA cap evades host restriction by IFIT family members. *Nature* 468:452–456. <http://dx.doi.org/10.1038/nature09489>.
 27. Sen GC, Sarkar SN. 2005. Hitching RIG to action. *Nat. Immunol.* 6:1074–1076. <http://dx.doi.org/10.1038/ni1105-1074>.
 28. Stark GR, Keer IM, Williams BR, Silverman RH, Schreiber RD. 1998. How cells respond to interferons. *Annu. Rev. Biochem.* 67:227–264. <http://dx.doi.org/10.1146/annurev.biochem.67.1.227>.
 29. Katze MG, He Y, Gale M, Jr. 2002. Viruses and interferon: a fight for supremacy. *Nat. Rev. Immunol.* 2:675–687. <http://dx.doi.org/10.1038/nri888>.
 30. Fujimura T, Esteban R. 2011. Cap-snatching mechanism in yeast L-A double-stranded RNA virus. *Proc. Natl. Acad. Sci. U. S. A.* 108:17667–17671. <http://dx.doi.org/10.1073/pnas.1111900108>.
 31. Sims AC, Tilton SC, Menachery VD, Gralinski LE, Schafer A, Matzke MM, Webb-Robertson BJ, Chang J, Luna ML, Long CE, Shukla AK, Bankhead AR, III, Burkett SE, Zornetzer G, Tseng CT, Metz TO, Pickles R, McWeeney S, Smith RD, Katze MG, Waters KM, Baric RS. 2013. Release of severe acute respiratory syndrome coronavirus nuclear import block enhances host transcription in human lung cells. *J. Virol.* 87:3885–3902. <http://dx.doi.org/10.1128/JVI.02520-12>.
 32. Frieman M, Yount B, Agnihothram S, Page C, Donaldson E, Roberts A, Vogel L, Woodruff B, Scorpio D, Subbarao K, Baric RS. 2012. Molecular determinants of severe acute respiratory syndrome coronavirus pathogenesis and virulence in young and aged mouse models of human disease. *J. Virol.* 86:884–897. <http://dx.doi.org/10.1128/JVI.05957-11>.
 33. Yount B, Curtis KM, Fritz EA, Hensley LE, Jahrling PB, Prentice E, Denison MR, Geisbert TW, Baric RS. 2003. Reverse genetics with a full-length infectious cDNA of severe acute respiratory syndrome coronavirus. *Proc. Natl. Acad. Sci. U. S. A.* 100:12995–13000. <http://dx.doi.org/10.1073/pnas.1735582100>.
 34. Roberts A, Deming D, Paddock CD, Cheng A, Yount B, Vogel L, Herman BD, Sheahan T, Heise M, Genrich GL, Zaki SR, Baric R, Subbarao K. 2007. A mouse-adapted SARS-coronavirus causes disease and mortality in BALB/c mice. *PLoS Pathog.* 3:e5. <http://dx.doi.org/10.1371/journal.ppat.0030005>.
 35. Li C, Bankhead A, III, Eisfeld AJ, Hatta Y, Jeng S, Chang JH, Aicher LD, Proll S, Ellis AL, Law GL, Waters KM, Neumann G, Katze MG, McWeeney S, Kawaoka Y. 2011. Host regulatory network response to infection with highly pathogenic H5N1 avian influenza virus. *J. Virol.* 85:10955–10967. <http://dx.doi.org/10.1128/JVI.05792-11>.
 36. Sheahan T, Whitmore A, Long K, Ferris M, Rockx B, Funkhouser W, Donaldson E, Gralinski L, Collier M, Heise M, Davis N, Johnston R, Baric RS. 2011. Successful vaccination strategies that protect aged mice from lethal challenge from influenza virus and heterologous severe acute respiratory syndrome coronavirus. *J. Virol.* 85:217–230. <http://dx.doi.org/10.1128/JVI.01805-10>.
 37. Trumpfheller C, Caskey M, Nchinda G, Longhi MP, Mizenina O, Huang Y, Schlesinger SJ, Colonna M, Steinman RM. 2008. The microbial mimic poly IC induces durable and protective CD4⁺ T cell immunity together with a dendritic cell targeted vaccine. *Proc. Natl. Acad. Sci. U. S. A.* 105:2574–2579. <http://dx.doi.org/10.1073/pnas.0711976105>.
 38. Zhang Q, Lai K, Xie J, Chen G, Zhong N. 2009. Does unrestrained single-chamber plethysmography provide a valid assessment of airway responsiveness in allergic BALB/c mice? *Respir. Res.* 10:61. <http://dx.doi.org/10.1186/1465-9921-10-61>.
 39. Hamelmann E, Schwarze J, Takeda K, Oshiba A, Larsen GL, Irvin CG, Gelfand EW. 1997. Noninvasive measurement of airway responsiveness in allergic mice using barometric plethysmography. *Am. J. Respir. Crit. Care Med.* 156:766–775. <http://dx.doi.org/10.1164/ajrccm.156.3.9606031>.
 40. Gralinski LE, Bankhead A, III, Jeng S, Menachery VD, Proll S, Belisle SE, Matzke M, Webb-Robertson BJ, Luna ML, Shukla AK, Ferris MT, Bolles M, Chang J, Aicher L, Waters KM, Smith RD, Metz TO, Law GL, Katze MG, McWeeney S, Baric RS. 2013. Mechanisms of severe acute respiratory syndrome coronavirus-induced acute lung injury. *mBio* 4:00271–13. <http://dx.doi.org/10.1128/mBio.00271-13>.
 41. Edgar R, Domrachev M, Lash AE. 2002. Gene Expr. Omnibus: NCBI gene expression and hybridization array data repository. *Nucleic Acids Res.* 30:207–210.
 42. Desmyter J, Melnick JL, Rawls WE. 1968. Defectiveness of interferon production and of rubella virus interference in a line of African green monkey kidney cells (Vero). *J. Virol.* 2:955–961.
 43. Zornetzer GA, Frieman MB, Rosenzweig E, Korh MJ, Page C, Baric RS, Katze MG. 2010. Transcriptomic analysis reveals a mechanism for a pre-fibrotic phenotype in STAT1 knockout mice during severe acute respiratory syndrome coronavirus infection. *J. Virol.* 84:11297–11309. <http://dx.doi.org/10.1128/JVI.01130-10>.
 44. Diamond MS, Farzan M. 2013. The broad-spectrum antiviral functions of IFIT and IFITM proteins. *Nat. Rev. Immunol.* 13:46–57. <http://dx.doi.org/10.1038/nri3344>.
 45. Gitlin L, Benoit L, Song C, Cella M, Gilfillan S, Holtzman MJ, Colonna M. 2010. Melanoma differentiation-associated gene 5 (MDA5) is involved in the innate immune response to *Paramyxoviridae* infection in vivo. *PLoS Pathog.* 6:e1000734. <http://dx.doi.org/10.1371/journal.ppat.1000734>.
 46. Züst R, Dong H, Li XF, Chang DC, Zhang B, Balakrishnan T, Toh YX, Jiang T, Li SH, Deng YQ, Ellis BR, Ellis EM, Poidinger M, Zolezzi F, Qin CF, Shi PY, Fink K. 2013. Rational design of a live attenuated dengue vaccine: 2'-O-methyltransferase mutants are highly attenuated and immunogenic in mice and macaques. *PLoS Pathog.* 9:e1003521. <http://dx.doi.org/10.1371/journal.ppat.1003521>.

47. Li SH, Dong H, Li XF, Xie X, Zhao H, Deng YQ, Wang XY, Ye Q, Zhu SY, Wang HJ, Zhang B, Leng QB, Zuest R, Qin ED, Qin CF, Shi PY. 2013. Rational design of a flavivirus vaccine by abolishing viral RNA 2'-O methylation. *J. Virol.* 87:5812–5819. <http://dx.doi.org/10.1128/JVI.02806-12>.
48. Rusinova I, Forster S, Yu S, Kannan A, Masse M, Cumming H, Chapman R, Hertzog PJ. 2013. Interferome v2.0: an updated database of annotated interferon-regulated genes. *Nucleic Acids Res.* 41:D1040–D1046. <http://dx.doi.org/10.1093/nar/gks1215>.
49. Fensterl V, Wetzel JL, Ramachandran S, Ogino T, Stohman SA, Bergmann CC, Diamond MS, Virgin HW, Sen GC. 2012. Interferon-induced Ifit2/ISG54 protects mice from lethal VSV neuropathogenesis. *PLoS Pathog.* 8:e1002712. <http://dx.doi.org/10.1371/journal.ppat.1002712>.
50. Bolles M, Deming D, Long K, Agnihothram S, Whitmore A, Ferris M, Funkhouser W, Gralinski L, Totura A, Heise M, Baric RS. 2011. A double-inactivated severe acute respiratory syndrome coronavirus vaccine provides incomplete protection in mice and induces increased eosinophilic proinflammatory pulmonary response upon challenge. *J. Virol.* 85:12201–12215. <http://dx.doi.org/10.1128/JVI.06048-11>.
51. Enjuanes L, DeDiego ML, Alvarez E, Deming D, Sheahan T, Baric R. 2008. Vaccines to prevent severe acute respiratory syndrome coronavirus-induced disease. *Virus Res.* 133:45–62. <http://dx.doi.org/10.1016/j.virusres.2007.01.021>.
52. Fett C, DeDiego ML, Regla-Nava JA, Enjuanes L, Perlman S. 2013. Complete protection against severe acute respiratory syndrome coronavirus-mediated lethal respiratory disease in aged mice by immunization with a mouse-adapted virus lacking E protein. *J. Virol.* 87:6551–6559. <http://dx.doi.org/10.1128/JVI.00087-13>.
53. Netland J, DeDiego ML, Zhao J, Fett C, Alvarez E, Nieto-Torres JL, Enjuanes L, Perlman S. 2010. Immunization with an attenuated severe acute respiratory syndrome coronavirus deleted in E protein protects against lethal respiratory disease. *Virology* 399:120–128. <http://dx.doi.org/10.1016/j.virol.2010.01.004>.
54. Graham RL, Becker MM, Eckerle LD, Bolles M, Denison MR, Baric RS. 2012. A live, impaired-fidelity coronavirus vaccine protects in an aged, immunocompromised mouse model of lethal disease. *Nat. Med.* 18:1820–1826. <http://dx.doi.org/10.1038/nm.2972>.
55. Ke M, Chen Y, Wu A, Sun Y, Su C, Wu H, Jin X, Tao J, Wang Y, Ma X, Pan JA, Guo D. 2012. Short peptides derived from the interaction domain of SARS coronavirus nonstructural protein nsp10 can suppress the 2'-O-methyltransferase activity of nsp10/nsp16 complex. *Virus Res.* 167:322–328. <http://dx.doi.org/10.1016/j.virusres.2012.05.017>.
56. Li J, Chorba JS, Whelan SP. 2007. Vesicular stomatitis viruses resistant to the methylase inhibitor sinefungin upregulate RNA synthesis and reveal mutations that affect mRNA cap methylation. *J. Virol.* 81:4104–4115. <http://dx.doi.org/10.1128/JVI.02681-06>.